Gabor depth imaging with topography

Yongwang Ma and Gary F. Margrave

ABSTRACT

Seismic depth imaging algorithms are usually designed to migrate seismic data recorded on a flat surface. However, real seismic data are not always recorded in this way but on topographic surfaces. If seismic imaging algorithms for seismic data acquired from flat surfaces are simply applied to migration of topographic seismic data, the resulting images may be totally wrong. To address the topography problem, we can transform irregular seismic data to a flat datum and use depth imaging algorithms for flat-datum data to image them. This will add some extra cost due to transforming topographic data to their flat-datum versions. A direct and preferred way of doing this is to modify algorithms for topographic seismic data imaging, without any data conversion or datuming. In this paper, we describe a method that adapts the Gabor imaging algorithm to a direct depth migration for seismic data recorded on a topographic surface.

INTRODUCTION

Since seismic data are not always recorded on flat surfaces, depth migration algorithms that can handle topographic seismic data are needed. Often, ordinary imaging methods (for flat-datum data) can be used to image topographic data, but extra considerations need to be taken to make flat-datum imaging algorithms work for topographic data. One of these methods is to transform recorded topographic data to a flat datum level above the highest source or receiver positions; then flat-datum imaging algorithms can be applied to get correct topographic images (e.g., Bevc, 1997; Beasley and Lynn, 1992). In other methods, we can modify the ordinary depth migration algorithms and use direct wavefield extrapolations from topographic surfaces, where receivers and sources sit, with careful arrangements of seismic data at depths (e.g., Reshef, 1991).

The Gabor imaging theory for flat datum migration is described in (Ma and Margrave, 2005). To improve the efficiency, adaptive partitioning algorithms (Grossman et al., 2002; Ma and Margrave, 2007a) have been developed. Runtime of the Gabor imaging method has been substantially reduced by using adaptive partitioning algorithms and spatial resampling theory (Margrave et al., 2006; Ma and Margrave, 2007b). To make the Gabor imaging algorithm more flexible, we bring this method to work for seismic shot records from topographic surfaces. We introduce a method, which extrapolates recorded seismic data (wavefields) directly from receiver and source positions along an irregular recording surface using the Gabor imaging algorithms. The application of the Gabor imaging algorithms in topographic migration is related to Reshef (1991) and Margrave and Yao (2000).

In the following sections, we describe the Gabor topographic migration method using the Model 94 datasets (Gray and Marfurt, 1995), synthetic datasets designed for testing topographic migration algorithms.

WAVEFIELD EXTRAPOLATION FROM TOPOGRAPHY

The Gabor imaging algorithm for flat-datum seismic data is formulated as (Ma and Margrave, 2006)

$$\psi(x, z+\Delta z, \omega) \approx \sum_{j\in\mathbb{Z}} \Omega_j(x) S_j(x) \int_{\mathbb{R}} \hat{\psi}(k_x, z, \omega) \hat{W}_j \left(k_j = \frac{\omega}{v_j}, k_x, \Delta z\right) \exp\left(-ik_x x\right) \mathrm{d}k_x \tag{1}$$

where ω is temporal frequency, k_x is transverse wavenumber, $\hat{\psi}(k_x, z, \omega)$ is the wavefield in depth z, wavefield extrapolator $\hat{W}_j$ extrapolates $\hat{\psi}(k_x, z, \omega)$ to a new depth $z + \Delta z$ (Δz is called the step size) and is defined as

$$\hat{W}_j = \exp\left(ik_j \Delta z\right). \tag{2}$$

The wavefield extrapolation using equation 1 is performed in partitions Ω_j; S_j is known as the split-step Fourier (Stoffa et al., 1990) correction in Ω_j.

In recursive depth marching schemes, the key role is played by the wavefield extrapolator $\hat{W}_j$, which drives the wavefield from depth to depth. An inspection of formula 2 shows that $\hat{W}_j$ is closely related to the depth step size Δz. If $\Delta z = 0$, $\hat{W}_j = \exp(0) = 1$. This relation can be used to specify where the wavefield should be extrapolated in the Gabor imaging method for topographic seismic data.

We set the starting point from a flat datum above all sources and receivers. As a result, there is a band of area (top flat, bottom rugged along topography) between the flat datum and the topography, where no physical waves are expected to propagate. The seismic wavefields (shot records) should only be extrapolated until the depth marching reaches the topographic surface where data (shot records) are recorded. This is also true for point sources modelled at various source positions. To specify where to extrapolate, we relate the extrapolator $\hat{W}_j$ to Δz. i.e.; when extrapolation is not needed, we set $\Delta z = 0$, and $\hat{W}_j = 1$, meaning no phase-shift will be applied. Otherwise, $\Delta z \neq 0$, phase-shift will be performed accordingly using equation 1.

The shot records, consisting of seismic traces, are recorded along the surface at different altitudes. When we extrapolate seismic wavefields from depth to depth, they are added in according to altitudes where they are recorded. i.e., seismic signals stored in these traces start to be extrapolated according to their altitudes related to receiver positions along topography.

Δz across the 2D profile is created as a 2D table (see Figure 1) and defined as

$$\Delta z = \begin{cases} 0 & \text{above topography,} \\ z_h, z_h \in (0, h) & \text{along topography,} \\ h & \text{below topography.} \end{cases} \tag{3}$$

where h is the full depth step size. Definition of Δz in equation 3 indicates extrapolations carried on in depths.

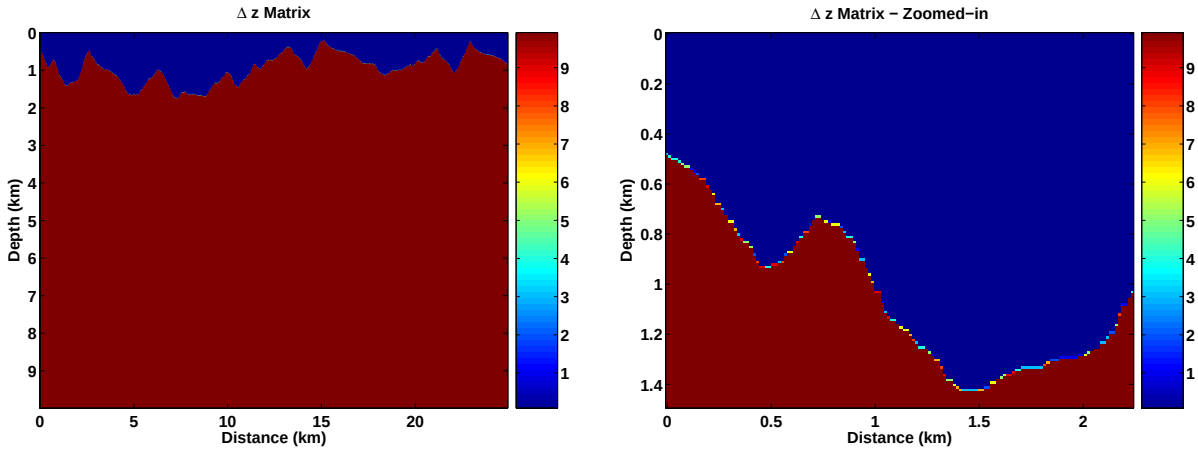

(a) (b)

FIG. 1. A 2D section of extrapolation step sizes for topographic imaging. (a) the full section, (b) zoomed-in on the upper left of the section. In (b), the small coloured boxes along the topographic surface indicates the z_h defined by equation 3. In (a), these z_h boxes are not discernible.

GABOR IMAGING WITH TOPOGRAPHY MODEL 94

Velocity Model 94

Model 94 (Gray and Marfurt, 1995) synthetic seismic datasets are used to test depth migration algorithms for topography. The velocity model is shown in Figure 2, which simulates the complex Canadian Foothills overthrust structures. The model dimensions are from left to right, 0 to 25 km and depth from 0 to 10 km. We can see that this model not only has very rapidly varying topography on the surface, but also has complex velocity structures beneath, which makes it quite challenging for depth migration algorithms.

Model 94 Dataset

The seismic datasets for Model 94 were created using 2D finite difference modelling codes (Gray and Marfurt, 1995). There are 278 shots, with a spatial interval of 90 m. The first shot position is at 0 m; there are 240 receivers in the first and the last shot spreads. Spreads roll in and out from the left to the right and the maximum number of receivers in a shot record is 480. Trace length is 2000 with time sampling interval of 4 ms. Receiver interval is 15 m. The full extrapolation step size in the vertical direction is $h = 10$ m.

The frequency band of the wavelet is obtained by analyzing a few seismic traces from

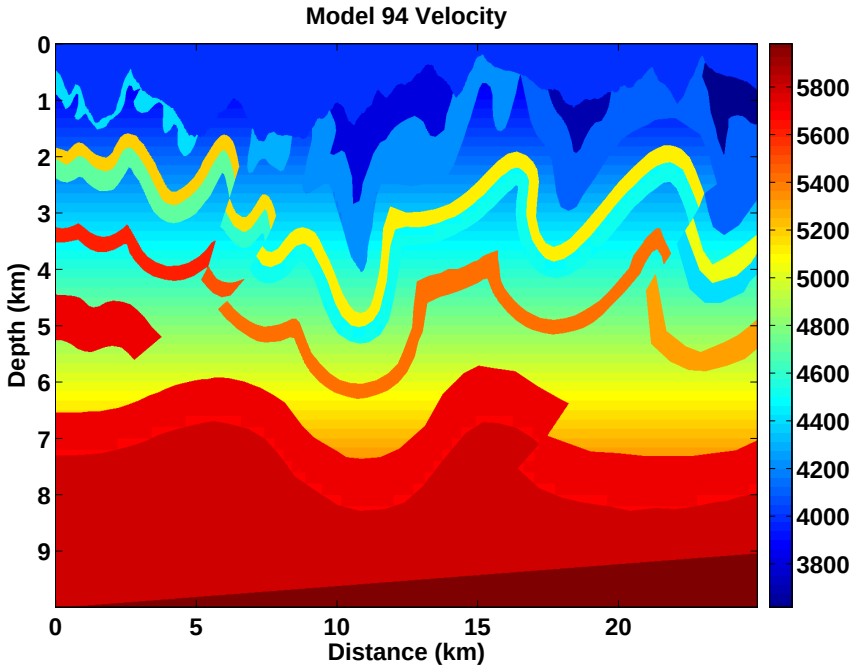

FIG. 2. Model 94 Velocity Model

the Model 94 datasets. We use an Ormsby wavelet with frequency limits of [0 10 30 50] Hz. Figure 3 shows the spectra of a few traces selected from the datasets.

Figure 4 (a) shows the first shot record on the left side, with source point at $x = 0$ m. Figure 4 (b) shows another shot record from the middle part.

Figures 5 (a) and (b) show the receiver elevations and the shot elevations along the topographic surface.

Imaging Examples with Model 94

Figure 6 (a) shows the imaging using the first shot record. We can see the topography is clearly shown in the image. Also, the first migrated section shows a little structure illuminated by the first shot. However, we see that there is a blackish (high amplitude) area in the shallow part. This is possibly caused by evanescent leaking during the spatial resampling of wavefields in frequency bands when extrapolating in the shallow part near the topographic surface. This is open for further research.

Figure 6 (b) shows the stacked imaging of the first 47 shot migrations. In this picture, we can see that some features of layers in the deeper part show up obviously.

If we add in more shot migrations, we can see in Figure 6 (c) that more and more structure comes into the picture. Another improvement is that the structure shown before is becoming more resolved.

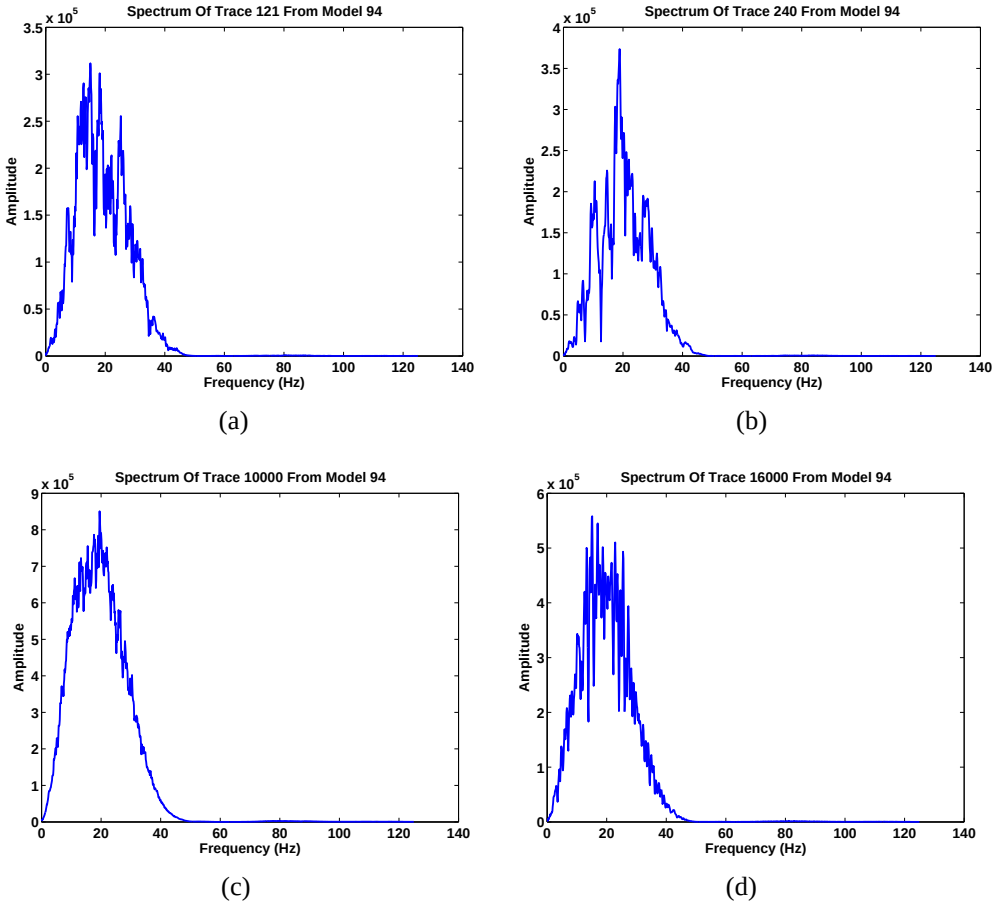

FIG. 3. The spectra of selected traces from Model 94 synthetic datasets.

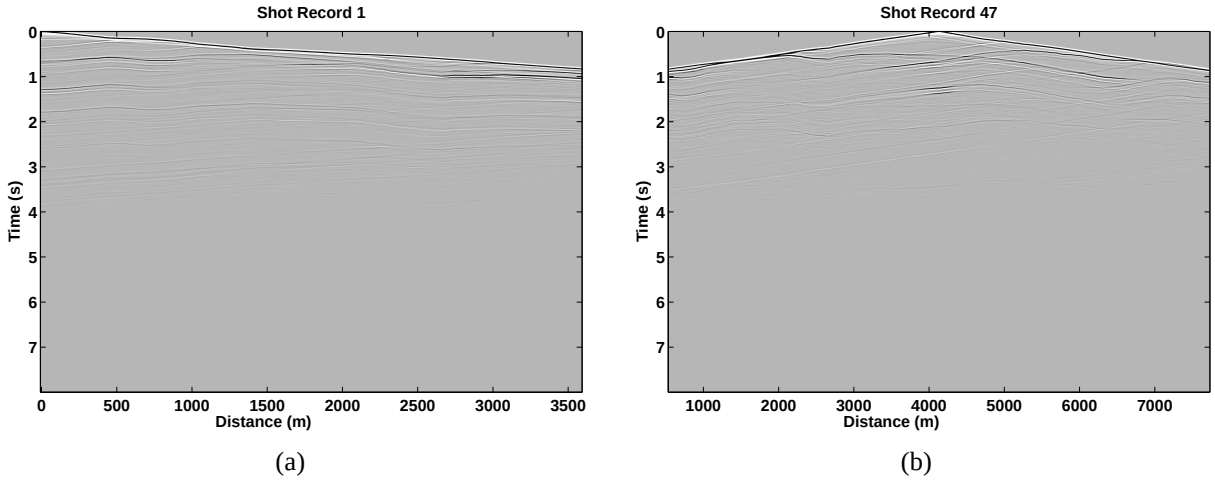

FIG. 4. Two shot records from Model 94 synthetic datasets. (a) The first shot record, (b) the 47th shot record.

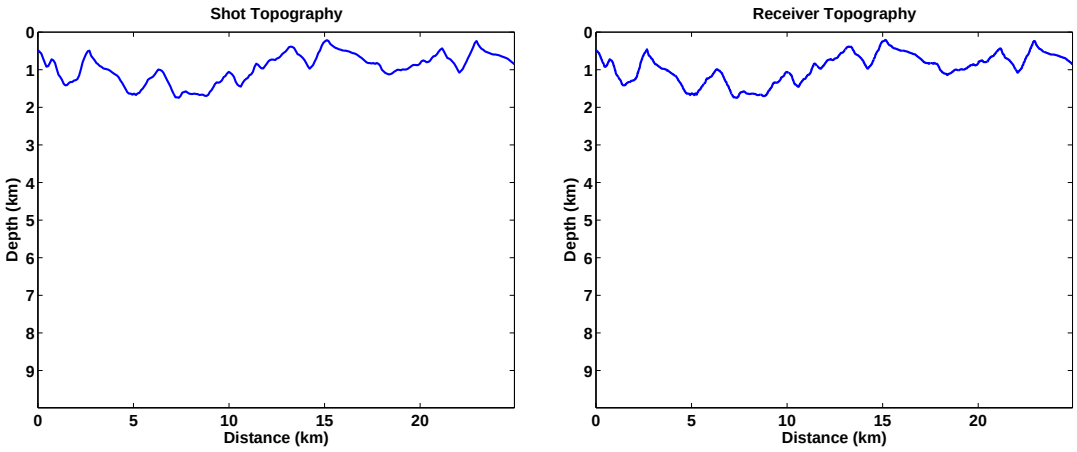

(a) (b)

FIG. 5. Shot and receiver positions on the topography surface in Model 94. (a) Shot positions, (b) receiver positions.

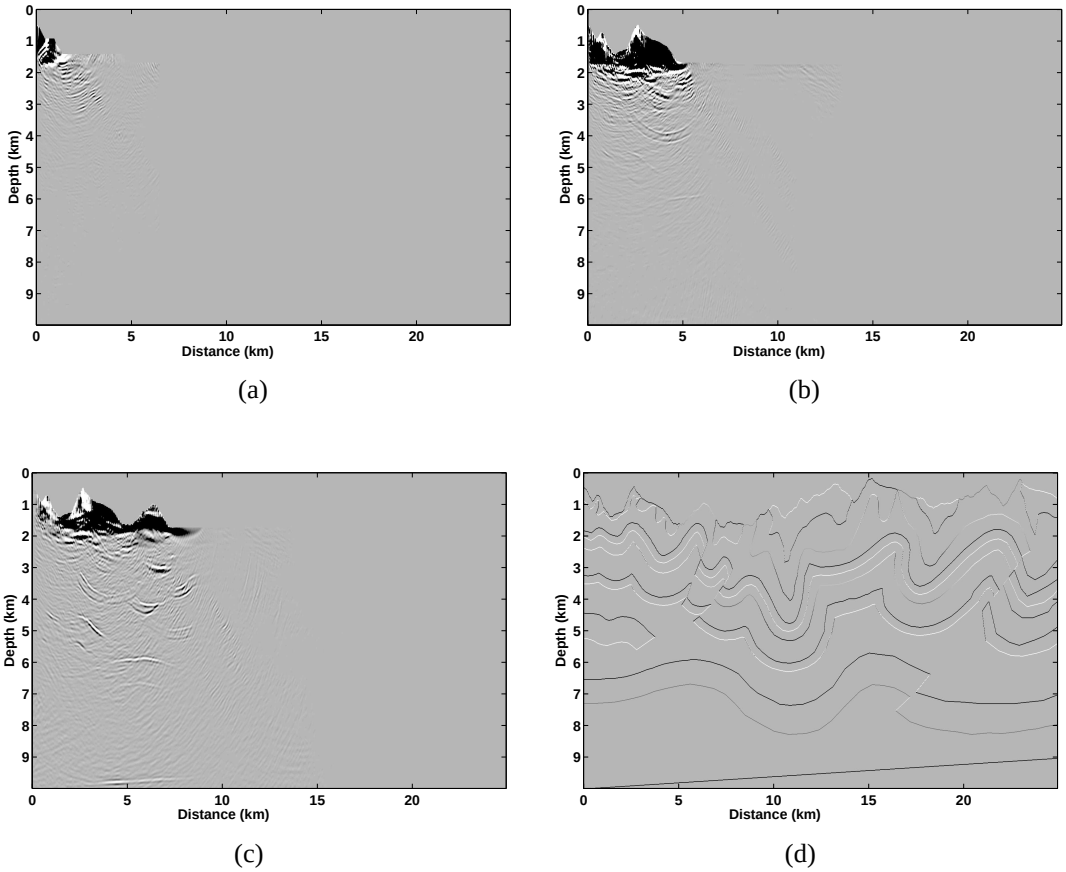

(a) (b)

(c) (d)

FIG. 6. Shot migrations from the Gabor imaging algorithms for topography seismic datasets of Model 94. (a) Migration of the first shot record, (b) migration of the first 47 shot records, (c) migration of the first 81 shot records, (d) the reflectivity image of Model 94.

Figure 6 (d) is the reflectivity image of Model 94. Comparing the partially imaged Model 94 with the reflectivity image, we can see that the Gabor imaging algorithm has obtained correct images of Model 94 though only partially done; which means that this topographic imaging method works, but not perfectly.

CONCLUSIONS

The Gabor imaging method for 2D depth migration has been made more efficient and flexible since it was developed within the CREWES project. At each stage, the performance of the Gabor imaging method was improved not only in imaging quality but also imaging speed. This imaging method has been made to work for topographic seismic data migration.

ACKNOWLEDGEMENTS

We wish to thank the Consortium of Research in Elastic Wave Exploration Seismology (CREWES) and its sponsors for financial support of this research. We thank the original contributors of the synthetic data sets used in this paper; they are Sam Gray, Gary Maclean and John Etgen. Thank Han-xing Lu for retrieving the topography and geometry information from the synthetic data sets for us. Thank David Henley for reviewing this paper.

REFERENCES

Beasley, C., and Lynn, W., 1992, The zero-velocity layer: Migration from irregular surfaces: Geophysics, **57**, 1435–1443.

Bevc, D., 1997, Flooding the topography: Wave-equation datuming of land data with rugged acquisition topography: Geophysics, **62**, 1558–1569.

Gray, S. H., and Marfurt, K. J., 1995, Migration from topography: Improve the near-surface image: Canadian Jorunal of Exploration Geophysics, **31**, 18–24.

Grossman, J. P., Margrave, G. F., and Lamoureux, M. P., 2002, Fast wavefield extrapolation by phase-shift in the nonuniform Gabor domain: CREWES Research Report, **14**.

Ma, Y., and Margrave, G. F., 2005, Prestack depth migration with the Gabor transform: CREWES Research Report, **17**.

Ma, Y., and Margrave, G. F., 2006, Prestack depth imaging with the Gabor transform: 76th Annual International Meeting, SEG, Expanded Abstracts, 2504–2507.

Ma, Y., and Margrave, G. F., 2007a, Adaptive Gabor imaging using the lateral position error criterion: 77th Annual International Meeting, SEG, Expanded Abstracts.

Ma, Y., and Margrave, G. F., 2007b, Fast Gabor imaging with the spatial resampling: CREWES Research Report, **19**.

Margrave, G., and Yao, Z., 2000, Downward extrapolation from topography with a laterally variable depth step: 2000 Annual International Meeting, SEG, Expanded Abstracts.

Margrave, G. F., Geiger, H. D., Al-Saleh, S. M., and Lamoureux, M. P., 2006, Improving explicit seismic depth migration with a stabilizing wiener filter and spatial resampling: Geophysics, **71**, No. 3, S111–S120.

Reshef, M., 1991, Depth migration from irregular surfaces with depth extrapolation methods: Geophysics, **56**, 119–122.

Stoffa, P. L., Fokkema, J. T., de Luna Freire, R. M., and Kessinger, W. P., 1990, Split-step Fourier migration: Geophysics, **55**, 410–421.